Geoenvironmental Disasters

RESEARCH Open Access

Effect of compaction condition on the water retention capacity, microstructure and its evolution during drying of compacted loess

Tao Xiao[1], Ping Li[1,2*], Zhenhui Pan[1] and Jiading Wang[1]

Abstract

To investigate the initial microstructure and water retention capacity of compacted loess molded under different compaction energy, the soil–water characteristic curves (SWCCs) and pore-size distribution curves (PSDs) of compacted loess specimens with different molding water contents or compaction energies were determined. Moreover, the PSDs of compacted loess specimens dried to different suctions were measured and the fractal dimensions of these specimens were examined to explore the microstructural evolution of compacted loess during drying. The results show that molding water content mainly affects the densities of macropores and mesopores, and compaction energy only affects the density of macropores. As the molding water content range of 16% to 20%, the AEV decreases with the increase of molding water content. The specimen with a lower molding water content has a larger slope of SWCC (or desorption rate). Compaction energy influences the water retention capacity of compacted loess in the low suction range (< 30 kPa). In response to suction increase, the PSD of compacted loess changes a little, while the fractal dimension increases with suction and there is a good linear relationship between them, indicating that the roughness of the pore surfaces is increasing during drying. This study provides new insight into the relationship between water retention capacity and pore structure of compacted loess and the microstructural evolution of compacted loess during drying, which is meaningful to the prevention of loess geological hazards.

Keywords: Compacted loess, Compaction condition, SWCC, PSD, Fractal dimension

Introduction

Loess soils are typically unsaturated and mainly distributed in arid and semi-arid areas (Dijkstra et al. 2014; Nan et al. 2021). It is common to use loess as building materials in local regions in the past. Recently, a series of land-creation projects have been carried out in the Loess Plateau of China to create land on which to build (Zhang et al. 2019; Xu et al. 2021). In these projects, rolling and tamping methods were used to remove the loess soils from mountain tops to valleys, thus a large number of fill slopes and fill foundations were produced. These fill slopes and fill foundations always experience considerable post-construction deformation (Zhu et al. 2019; Zhang et al. 2022). In addition, natural loess has large void ratio and strong water sensitivity. These characteristics can be eliminated by compaction to increase the soil density. Therefore, it is of great importance to study the influence of compaction condition on the mechanical and hydraulic properties of compacted loess. Previous studies have shown that dry density (or compaction energy) and molding water content are the two most key parameters affecting the properties of compacted loess statically prepared; they influence the soil behavior by changing the soil structure (Romero et al. 1999; Hou et al. 2020; Zhang et al. 2021).

The soil–water characteristic curve (SWCC) depicts the relationship between soil suction and water content

*Correspondence: liping_dzxx@nwu.edu.cn

[1] State Key Laboratory of Continental Dynamics, Department of Geology, Northwest University, Xi'an 710069, China
Full list of author information is available at the end of the article

(or energy of saturation), providing an understanding of the distribution of water in the voids. The SWCC is an important parameter to characterize the water retention capacity of unsaturated soil, and has great practical significance for the implementation of unsaturated soil mechanics (Ng et al. 2016a; Tu and Vanapalli 2016; Gao et al. 2021a, b). For instance, the SWCC is required for modelling the water flow and contaminant transport in unsaturated soil, as well as for estimating the field capacity and soil aggregate stability. The measurement of SWCC is very laborious and time-consuming, and depends on the method or instrument used to measure suctions, the operator's ability and experience. For this reason, research on the water retention capacity of loess is not as extensive as that on the strength or collapsibility, and not much measured data were reported (Huang et al. 2010; Muñoz-Castelblanco et al. 2012; Wang et al. 2019; Zhang et al. 2021). For example, Huang et al. (2010) compared the predictions of two PTFs (Pedo-Transfer Functions) for estimating the SWCC from the particle-size distribution (PSD) using a dataset involving 258 natural loess samples. Muñoz-Castelblanco et al. (2012) presented the SWCC of a natural loess from Northern France with no hysteresis around the natural water content and two hysteresis loops on both the dry and wet sides of the curve. Meanwhile, their results showed that the water retention is governed by capillarity in the largest pores between clean grains, whereas clay adsorption becomes dominant in the smallest pores. Wang et al. (2019) investigated the influence of soluble salt on the SWCC of Ili loess and proposed a SWCC equation with the salt content as a variable based on the Gardner model. Cheng et al. (2020a) studied the effect of temperature on the SWCC of compacted loess, and concluded that the water retention capacity of compacted loess decreases with the increase of temperature. Ng et al. (2016b) measured and compared the SWCCs and PSDs of compacted loess and investigate the volume change behavior of both loess soils during drying and wetting process. While the compacted loess specimens were nominally the same in their study, and the water content and dry density of compacted loess are similar to that of intact loess. The effects of molding water content and compaction energy on the water retention capacity of compacted loess were rarely investigated.

Soils in the natural environment will inevitably be affected by drying or evaporation. A number of studies suggest that the soil microstructure may change during water evaporation, which would result in a variety of geotechnical and geological problems (Cheng et al. 2020b; Ying et al. 2021). For example, the hydraulic properties of soil (the water retention capacity, permeability, etc.) can be considerably modified, according to Chertkov (2000) and Tang et al. (2021). Besides, the cracks caused by drying contribute to rainfall infiltration, which may induce slope failure (Gao et al 2021a, b). Several studies showed that water evaporation is one of the most important inducers for the formation of vertical joints in natural loess (Li et al. 2020a; Feng et al. 2021). However, little attention has been paid to the evolution of microstructure during the drying process for compacted loess.

For the above reasons, to investigate the microstructure and water retention capacity of compacted loess and its microstructural evolution during drying is particularly necessary. In this study, the objectives are: (1) to investigate the initial microstructure and water retention property of compacted loess with different molding water contents or compaction energies; (2) to explore the relationship between the initial microstructure and water retention capacity of compacted loess; (3) to examine the microstructural evolution of compacted loess during drying.

Material and methods

Material

The loess soil tested was taken from Luochuan, China. The physical properties of this soil are summarized in Table 1. The liquid limit and plasticity limit of the loess soil are 28.2% and 17.7%, respectively. According to the Unified Soil Classification System (USCS) and the method proposed by Gibbs and Holland (1960), this soil can be classified as 'CL' and 'Silty loess' (see Fig. 1). The optimum water content is approximately 18% and the maximum dry density is 1.75 g/cm^3, see Fig. 2. The mineral composition determined by using X-ray diffraction shows that the soil consists mainly of quartz, calcite, albite, kaolinite and biotite.

To prepare compacted specimens, the oven-dried soils were screened with a 2 mm sieve and mixed with a predetermined amount of distilled water to achieve the target gravimetric water content, i.e., 16%, 18% or 20%. The wet soils were packed in plastic bags and kept in humid

Table 1 Physical properties of the loess soil studied

Property	Value
In-situ water content (%)	9.9
In-situ density (g/cm^3)	1.46
Specific gravity, G_s	2.71
Liquid limit, w_L (%)	28.2
Plastic limit, w_P (%)	17.7
Plastic index, I_p	10.5
Maximum dry density (g/cm^3)	1.75
Optimum water content (%)	18

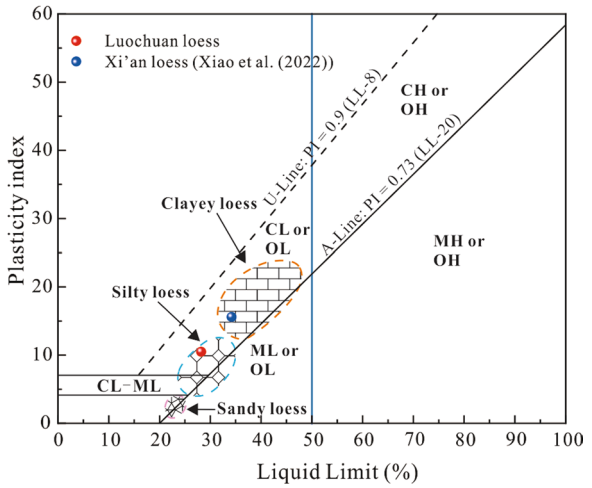

Fig. 1 Soil classification chart for the loess studied according to the USCS and the method proposed by Gibbs and Holland (1960)

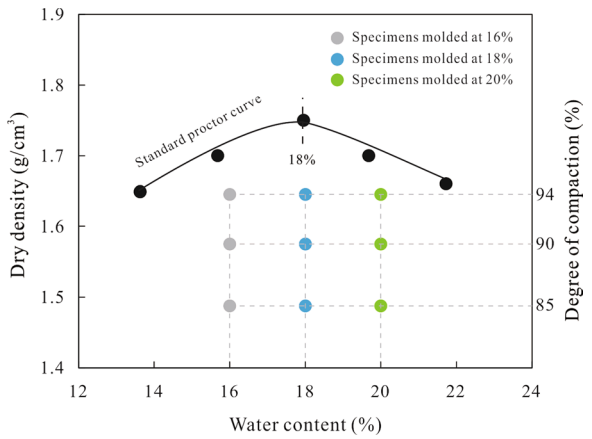

Fig. 2 Compaction curve of loess soil studied

chambers for water equalization. Then, the wet soils were compacted statically using a self-designed sample preparation equipment to reach the target dry density or compaction degree, i.e., 85%, 90% or 94%. In total, nine compacted specimens and their parallel specimens were prepared, their water contents or compaction degrees are different. The details of the specimens are summarized in Table 2. Their SWCCs were measured subsequently using the axis translation technique. To study the effect of drying or suction increase on the microstructure of compacted loess, four groups of compacted loess specimens (WR16%-CD85%, WR18%-CD85%, WR20%-CD85%, WR18%-CD94%, WC means molding water content, CD means compaction degree) were prepared. These specimens were saturated and then dried to different levels

Table 2 Details of the loess specimens

Specimen	Molding water content (%)	Compaction degree (%)	Dry density (g/cm^3)	Void ratio
WR16%-CD85%	16	85	1.4875	0.8218
WR16%-CD90%	16	90	1.5750	0.7206
WR16%-CD94%	16	94	1.6450	0.6474
WR18%-CD85%	18	85	1.4875	0.8218
WR18%-CD90%	18	90	1.5750	0.7206
WR18%-CD94%	18	94	1.6450	0.6474
WR20%-CD85%	20	85	1.4875	0.8218
WR20%-CD90%	20	90	1.5750	0.7206
WR20%-CD94%	20	94	1.6450	0.6474

of suction. As the equilibrium was achieved, the PSD of each specimen at a specific level of suction was determined by mercury intrusion porosimetry (MIP).

Methods

SWCC measurement

The SWCCs of compacted loess specimens were measured using a 15-bar pressure plate extractor. The prepared compacted loess specimens with a diameter of 5.3 mm and a height of 1 cm were first saturated in a cylinder under the vacuum condition for 48 h, and then placed on the ceramic disk that was also saturated in the pressure chamber. Afterward, air pressure was applied to the chamber, the specimens were brought to a suction that was equal to the applied air pressure. The air pressure applied to the chamber followed the order of 1, 3, 6, 9, 25, 50, 75, 100, 150, 200, 300, 400, 500, 700, 900, 1100 kPa. As an increasing air pressure was applied, water was discharged from the specimens until the equilibrium was reached. The water flowing from the chamber was recorded daily at each suction. The equilibrium state was considered to be reached when the outflow rate was less than or equal to 0.144 mL/d, according to Ye et al. (2019). It took 4–14 days to reach the equilibrium state in response to a suction increment. This time varied depending on the suction (or air pressure) applied to the specimens. The higher the suction was, the longer the time was required for the equilibrium state; that is because the soil permeability decreases with suction dramatically, the time for drainage of water increases with

suction (Jiang et al. 2017; Zhang et al. 2021). After reaching the equilibrium, the specimens were taken out of the chamber and weighed immediately for determining their water contents.

Microstructure measurement

The initial pore structure and change in the pore structure of compacted loess induced by drying or suction increase were investigated by using the MIP technique. Before the intrusion of mercury, each specimen that was 1 cm × 1 cm × 1 cm in size was dried by using the freezing drying method. The porosimeter used could apply a pressure ranging between 0.5 and 60,000 psi to the mercury, the corresponding range of entrance diameter was 3 nm–360 μm according to the Young–Laplace's equation.

Experimental results and discussion

Initial pore structure of compacted loess

Figure 3a–c presents the PSDs of compacted loess specimens with the same compaction energy and different molding water contents, and the curves of compacted loess specimens with the same molding water content and different compaction degrees are presented in Fig. 3d–f. The pores in compacted loess are divided into three groups according to the pore diameter, i.e., micropores ($d \leq 200$ nm), mesopores (200 nm $< d \leq 3000$ nm) and macropores ($d > 3000$ nm). This classification is adopted to facilitate the description of the PSD variation due to changes in molding water content or compaction energy. The boundary between micropores and mesopores is 200 nm, which is identical to the boundary diameter between intra-aggregate pores and inter-aggregate pores (Xiao et al. 2022).

It is worth noting that the bimodal characteristic of the PSD is not modified no matter whether the specimen was molded at dry side or wet side of the optimum water content, all curves have two peaks. In Fig. 3a–c, at the same molding water content, the PSD of macropores varies a lot while that of micropores or mesopores changes a little with the increase of compaction energy. It can be seen that as compaction energy increases from 85 to 90% or 94%, not only the peak density decreases, the corresponding pore diameter in the range of macropores (i.e., the dominant diameter of inter-aggregate pores) reduces from 6000 nm to approximately 4000 nm or 3000 nm (see Fig. 3a). Moreover, the PSD variation of compacted loess due to changes in compaction energy is similar to that during consolidation and shearing, as reported by Li et al. (2020b); that is, the PSD of inter-aggregate pores is compressed to the left, while that of intra-aggregate pores maintains unchanged. As shown in Fig. 3d–f, at the same compaction energy, the density of macropores decreases with the increase of molding water content, meanwhile the density of mesopores increases significantly; however, there is no remarkable change in the dominant diameter of inter-aggregate pores.

Figure 4 summarizes the void ratios of micropores, mesopores and macropores (e_{micro}, e_{meso}, e_{macro}) of all compacted loess specimens. It can be seen that e_{micro} rarely changes as compaction condition varies, being consistent with that described above. At a given compaction energy, e_{macro} decreases and e_{meso} increases with the increasing molding water content. At a given molding water content, only e_{macro} decreases with the increase of compaction energy. As shown in Fig. 4, at the compaction degree of 85%, as molding water content increases from 16 to 20%, e_{macro} decreases from 0.372 to 0.343 and e_{meso} increases from 0.230 to 0.242. At the molding water content of 16%, as compaction degree increases from 85 to 94%, e_{macro} decreases from 0.372 to 0.168.

It is widely acknowledged that different compaction conditions (mainly refer to molding water content and compaction energy for static compaction) produce different soil microstructures (Romero et al. 1999; Alonso et al. 2013; Li et al. 2016; Cheng et al. 2020b). A microstructural state variable, ξ_m, introduced by Alonso et al. (2013) can be used to further analyze the microstructural variation of compacted loess; $\xi_m = e_m / e_{total}$, where, e_{total} is the total void ratio, and e_{total} is the sum of the void ratio of intra-aggregate pores (e_m) and the void ratio of inter-aggregate pores (e_M) (Alonso et al. 2013). Since the micropores defined in this study are actually intra-aggregate pores, the boundary diameter between micropores and mesopores is identical to that between intra-aggregate pores and inter-aggregate pores, the microstructural state variable of each specimen can be obtained from its PSD. The ξ_m values of nine compacted loess specimens are summarized in Fig. 5. It can be observed that ξ_m increases with the increase of compaction energy at any molding water content. While ξ_m does not have a clear trend in response to the increase of molding water content. For example, at the compaction degree of 85%, ξ_m is almost unchanged; while at the compaction degree of 90%, ξ_m increases first and then decreases with the increase of molding water content. That is different from the observation of Cheng et al. (2020b) on a compacted silt; they found that ξ_m increases with the increasing molding water content, indicating that intra-aggregate pores are increased.

SWCC

The SWCCs of compacted loess specimens are depicted in Fig. 6. The curves are shown in terms of gravimetric water content. According to Vanapalli et al. (1996), the desaturation of a soil is commonly divided into

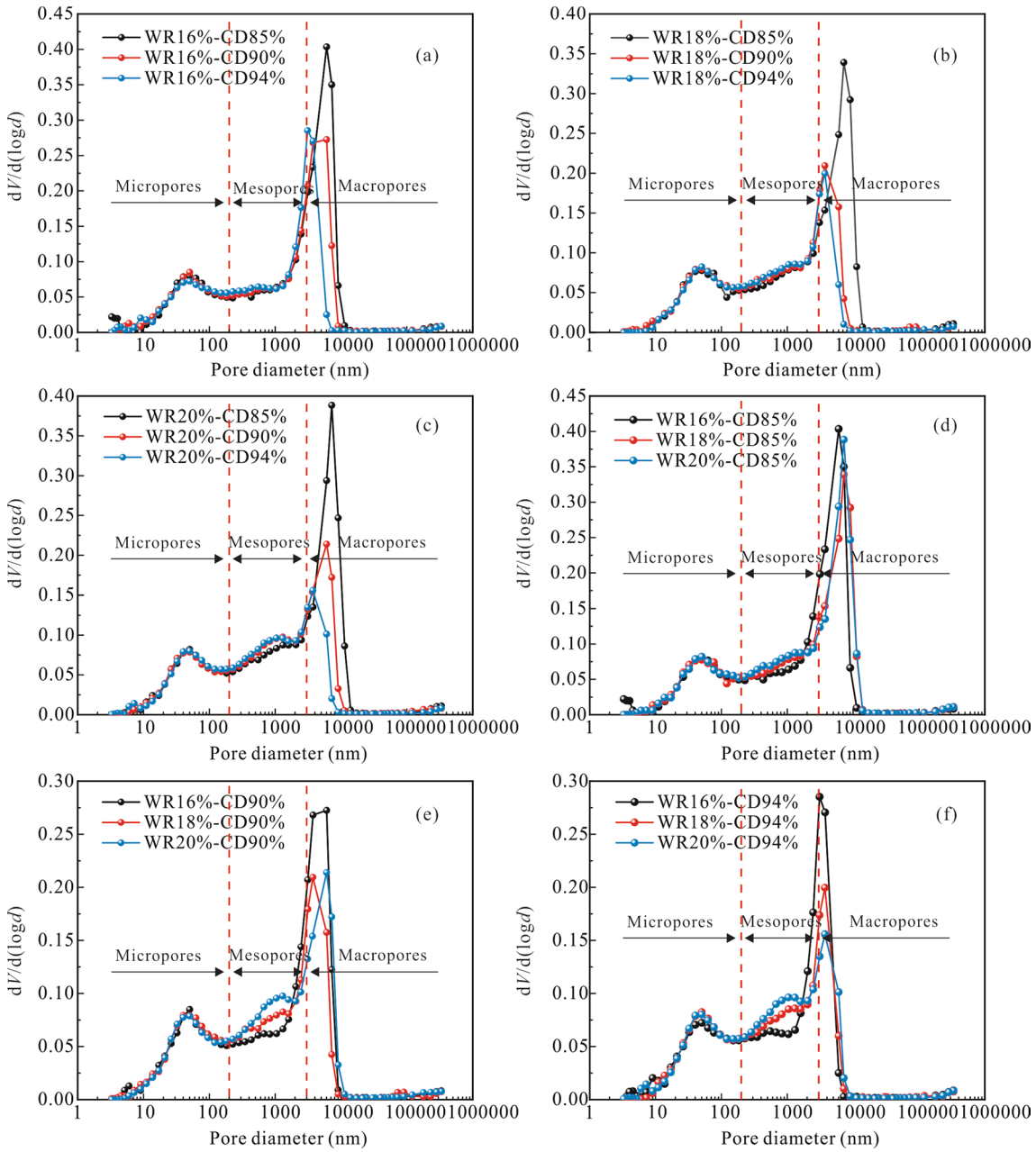

Fig. 3 PSDs of compacted loess specimens compacted at molding water contents of **a** 16%, **b** 18%, **c** 20% and compaction degrees of **d** 85% **e** 90% **f** 94%

three stages, which can be delineated by three zones on the drying SWCC, i.e., boundary effect zone, transition zone and residual zone. It shows in Fig. 6a–c that compaction energy has significant influence on the boundary effect zone. An increase in compaction energy means a decrease in void ratio. Hence, at the same molding water content, the greater the compaction degree of compacted loess specimen, the smaller the saturated gravimetric water content and air-entry value (AEV). This observation is consistent with the viewpoints of many scholars (e.g., Vanapalli et al. 1996; Birle et al. 2008). At the same molding water content, the SWCCs of compacted loess specimens with different compaction degrees tend to converge together when suction is higher than 30 kPa (see Fig. 6a–c). It suggests that compaction energy has little effect on

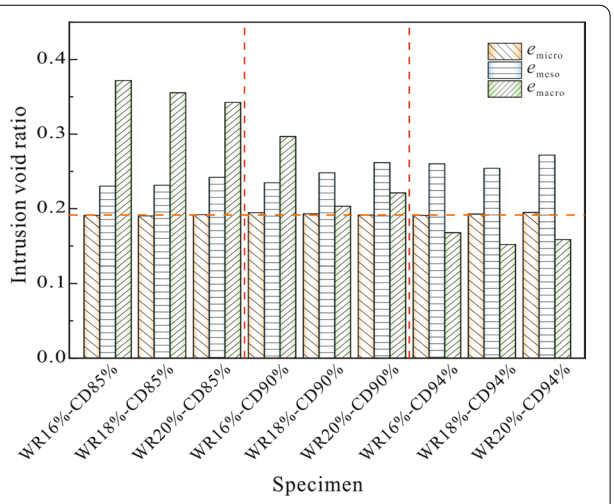

Fig. 4 Summary of e_{macro}, e_{meso}, e_{micro} of compacted loess specimens

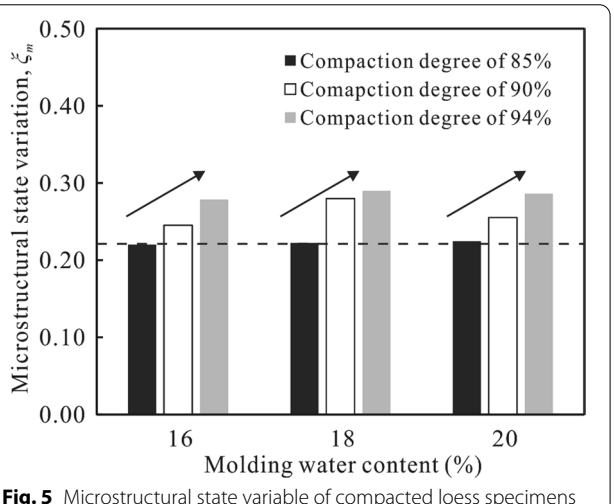

Fig. 5 Microstructural state variable of compacted loess specimens

the water retention capacity of compacted loess when suction exceeds 30 kPa. This result is similar to that obtained by Romero et al. (1999), Sreedeep and However (2006); they suggested that the water retention property of compacted soil is not affected by compaction energy and molding water content when suction exceeds a certain value. In addition, it is shown in many studies that compaction condition, wetting–drying action, freezing–thawing action, etc., only affect the SWCC in the low suction range, while the SWCC in the high suction range depends on the soil nature (such as the GSD and mineral composition) (Birle et al. 2008; Hou et al. 2020).

Figure 6e–f compares the SWCCs of compacted loess specimens with different molding water contents. It is observed that at the same compaction degree, compacted loess specimens have the same saturated gravimetric water content, that is understandable since they have the same void ratio. As molding water content increases, the AEV of compacted loess reduces slightly; for example, at the compaction degree of 85%, as molding water content increases, the AEV decreases from 10 to 8 kPa or 5 kPa (see Fig. 6e). This coincides with the results of Romero et al. (1999), Vanapalli et al. (1999) and Jiang et al. (2017). They thought it could be because the specimen with a higher molding water content has more macropores among aggregates since it has more aggregates. However, the pore structure measurement results show that macropores do not increase with the increase of molding water content (see Fig. 4). For this reason, it should be recognized that the AEV is related to the maximum diameter of pores in the specimen, which may not be accurately determined by MIP since too large pores (greater than 360 μm theoretically) can not be detected by MIP (Vanapalli et al. 1996). Moreover, the SWCCs of compacted loess specimens with the same compaction degree intersect at a suction, above which the curve of the specimen with a lower molding water content is below that of the specimen with a higher molding water content. It suggests that the latter has a smaller desorption rate and a higher water retention capacity than the former at the same suction.

The relationship between SWCC and initial pore structure

The equation proposed by van Genutchen (1980) was used to fit the SWCC data obtained in this study:

$$\theta = \theta_r + \frac{\theta_s - \theta_r}{[1+(\alpha s)^n]^m} \quad (1)$$

where, θ is the volumetric water content; θ_s is the saturated volumetric water content; θ_r is the residual volumetric water content; s is the suction; α, m and n are fitting parameters, α relates to the inverse of AEV; that is to say, α increases with the decrease of AEV.

Figure 7 presents the correlations between the SWCC fitting parameters (α, m, n), microstructural parameters (e_{total}, e_{macro}, e_{meso}, e_{micro}, ξ_m) and compaction condition (dry density, molding water content) obtained on the basis of multivariate statistical analysis. The closer the correlation coefficient to 1, the stronger the correlation. On the one hand, it can be observed that, α is negatively correlated with dry density while the coefficient is only −0.40. On the other hand, α is positively correlated with molding water content, with a correlation coefficient of 0.86. That is consistent with the observation that the AEV reduces slightly with the increase of molding water content. The fitting parameter m is negatively correlated with molding water content, with

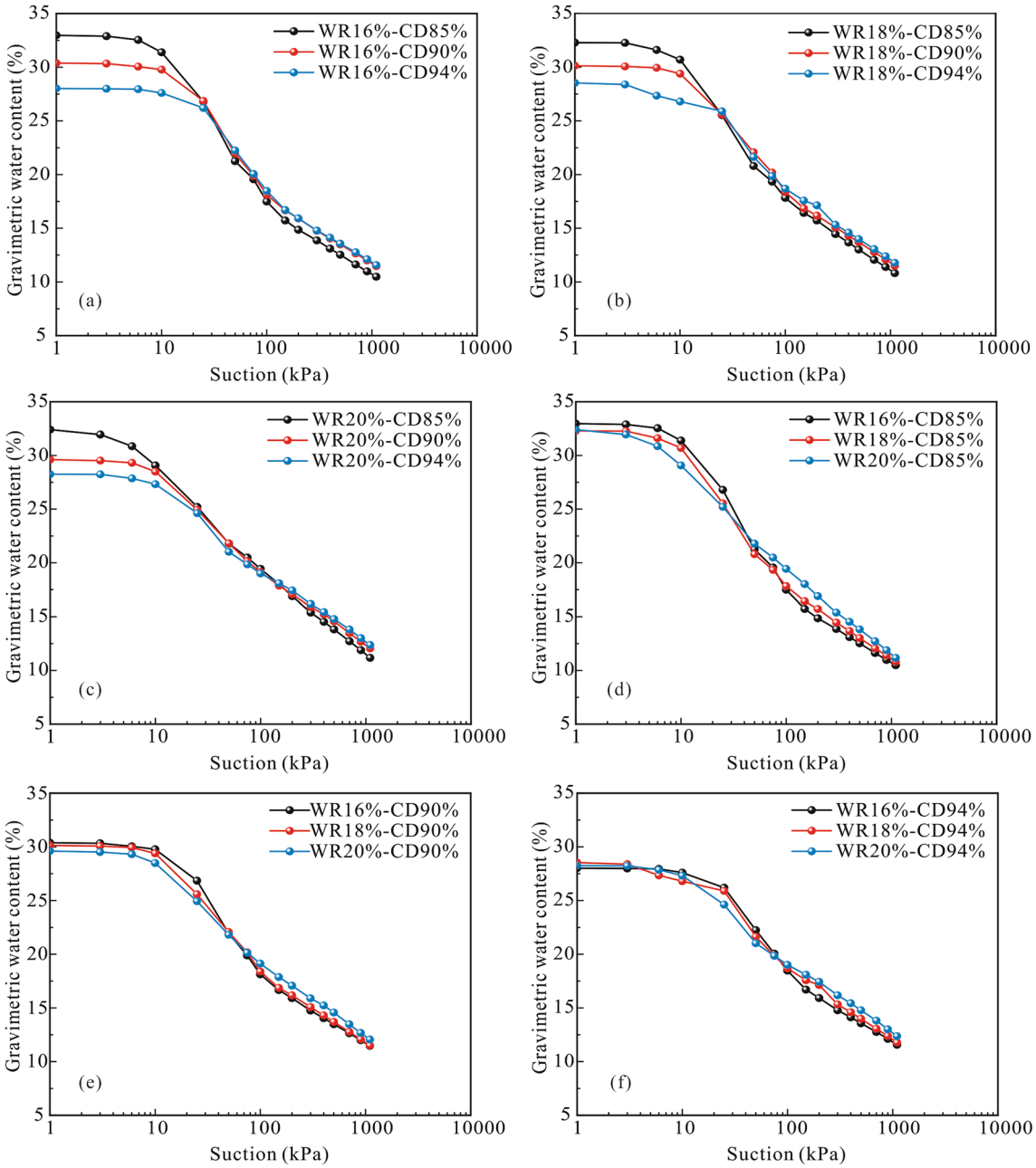

Fig. 6 SWCCs of compacted loess specimens compacted at molding water contents of **a** 16%, **b** 18%, **c** 20% and compaction degrees of **d** 85% **e** 90% **f** 94%

a correlation coefficient of −0.87. These suggest that the AEV and the shape of SWCC of compacted loess depend mainly on molding water content. That is different from the result of Zhao et al. (2017), they showed that void ratio or dry density has more significant effect on the shape of SWCC. It is worth noting that dry density is negatively correlated with e_{total} and e_{macro}, and there is a close relationship between molding water content and e_{meso}, and there is no significant connection found between e_{micro} and molding water content or dry density.

Microstructural evolution of compacted loess during drying

The PSDs of compacted loess specimens with different compaction degrees or molding water contents dried to

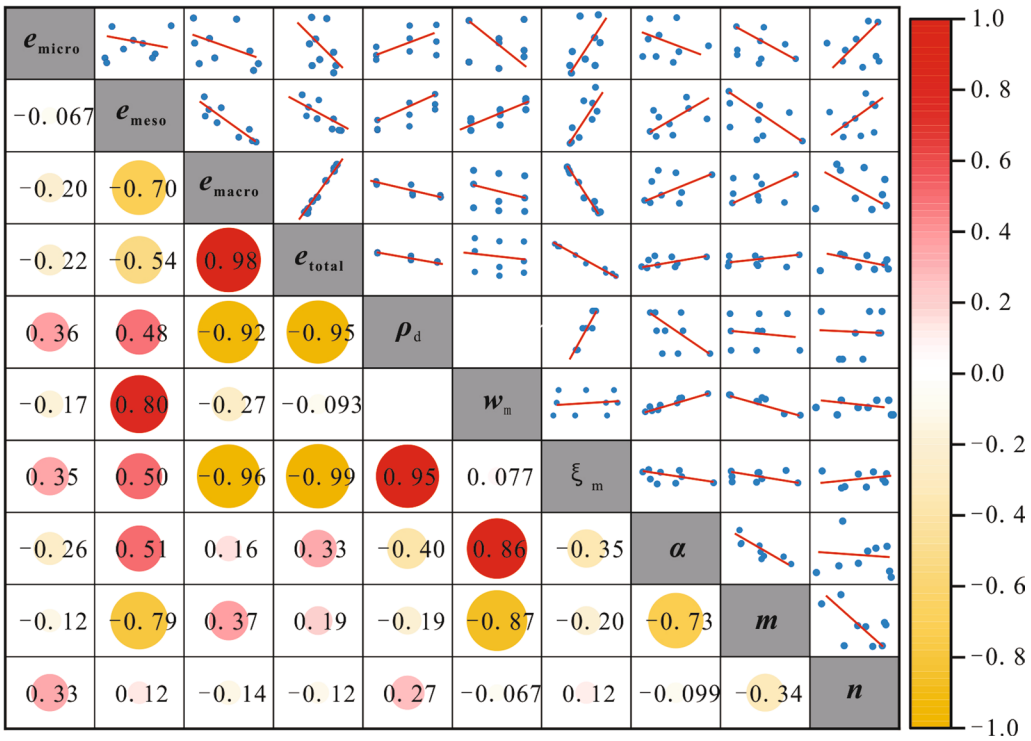

Fig. 7 Pearson's correlation analysis

six suctions (i.e., 3, 6, 50, 100, 200 and 400 kPa) are presented in Fig. 8. Similarly, drying or suction increase does not modify the bimodal characteristic of the PSD of compacted loess. The densities of mesopores and micropores in compacted loess specimens are little varied, and changes in the density of macropores are notable. This is similar to the observation of Cai et al. (2020) on a compacted red soil. Their results showed that intra-aggregate pores are almost unchanged during drying, while the density of inter-aggregate pores is affected evidently; the dominant diameter of inter-aggregate pores increases gradually with the increase of suction, meanwhile, the peak density corresponding to the dominant diameter of inter-aggregate pores grows during drying. In comparison, a clear trend could not be identified for the density of macropores from the results of this study, see Fig. 8. That is to say, the effect of drying or suction increase on the PSD of compacted loess under null pressure condition is weak and uncertain. This difference might be due to the difference in soil type. Red soil is a clayey soil, while the loess studied in this paper is a silt, the former soil is more sensitive to suction change. The study carried out by Fu et al. (2011) showed that during drying or wetting, the volumetric change of soil was very small in the low suction range, about 0.5% of the total volume. In addition, Hou et al. (2020) and Li (2021) reported that under the null pressure condition, the volume change of compacted loess is very small during either drying or wetting.

The variations of the void ratios of three pore families (micropores, mesopores and macropores) due to suction increase are presented in Fig. 9. It can be seen that as suction increases, the void ratios of micropores and mesopores are almost unchanged, and changes in the void ratio of macropores are obvious relatively. This further illustrates that larger pores are more sensitive to suction change. In addition, the total intrusion void ratios of specimens at different suctions are close (see Fig. 8d, 9b). Ying et al. (2021) also found that the variation of the void ratio of macropores in a lime-treated silt was relatively obvious while the total intrusion void ratio is basically unchanged with the increasing suction during drying.

Effect of drying on the fractal dimension of compacted loess

The fractal dimension is an important parameter that can be used to quantitatively characterize the complexity or roughness of the pore surfaces in porous media (Zhang et al. 1995). Several models have been proposed to determine the fractal dimension of soil as its PSD is known. One of the models, proposed by Zhang et al. (1995),

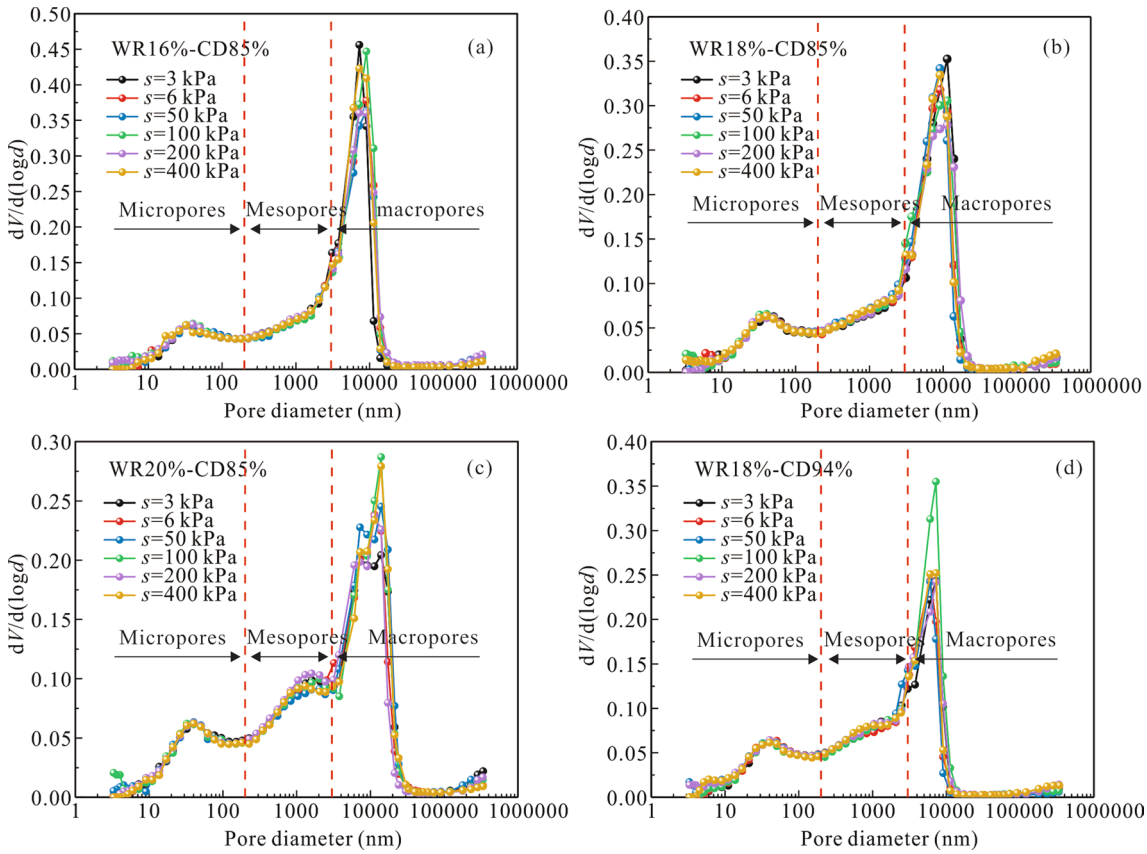

Fig. 8 PSDs of compacted loess specimens at different suctions (**a** WR16%-CD85%, **b** WR18%-CD85%, **c** WR20%-CD85%, **d** WR18%-CD94%)

assumes that in the process of mercury intrusion, the work done by the applied pressure on mercury is equal to the increase in the surface energy of mercury. The fractal dimension can be determined following the equations below:

$$\ln\left(W_n/r_n^2\right) = D_f lnQ_n + C \tag{2}$$

$$W_n = \sum_{i=1}^{n} P_i \Delta V_i \tag{3}$$

$$Q_n = V_n^{1/3}/r_n \tag{4}$$

where, W_n is the cumulative surface energy; V_n is the cumulative intrusion volume of the nth intrusion; Q_n is the function of pore radius (r_n) and V_n; P_i and V_i are the intrusion pressure and the corresponding volume during the ith intrusion; C is a constant associated with the surface tension and contact angle between soil particle and mercury; D_f is the fractal dimension.

Figure 10 presents how the fractal dimensions of specimens at different suctions were determined. It can be seen that the relationship between $\ln(Q_n)$ and $\ln(W_n/r_n^2)$ is linear, with a slope basically unchanged in the whole measurable range of pore diameter. The $\ln(Q_n)$–$\ln(W_n/r_n^2)$ curve can be well fitted by a straight line, with the deviation parameter greater than 0.99; the slope of the straight line is the fractal dimension of compacted loess specimen according to Eq. 1. It means that there is only one fractal interval in the whole measurable range of pore diameter; in other words, there is only one fractal dimension. It can be found in Fig. 10 that the slope of the straight line increases gradually with the increase of suction. That is to say, the fractal dimension of compacted loess is increasing in response to suction increase, the roughness of the pore surfaces is increasing during drying (Zhang et al. 1995; Sun et al. 2020). As shown in Fig. 8, changes in the PSD of compacted loess are not significant. However, when using the fractal dimension to quantitatively characterize the microstructural evolution of compacted loess, it is evidently shown that the roughness of the pore surfaces or complexity of the pore structure increases with the increase of suction during drying. From this point of view, the fractal dimension can be a supplement to the PSD; upon the analysis of both of

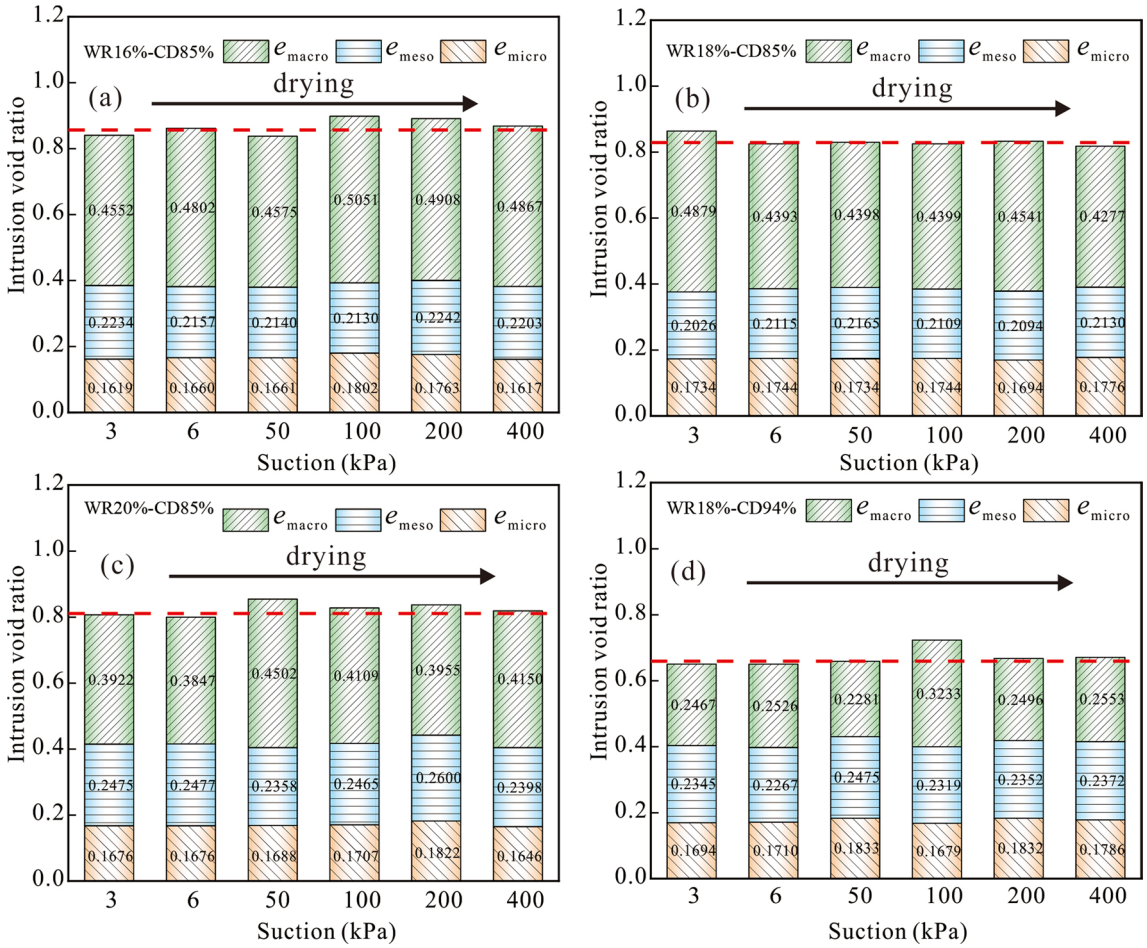

Fig. 9 Variations of the void ratios of three pore families in **a** WR16%-CD85%; **b** WR18%-CD85%; **c** WR 20%-CD85%; **d** WR18%-CD94%

them, the microstructural evolution of compacted loess could be interpreted comprehensively. It also suggests that although the suction increase or drying has a little effect on the pore size in compacted loess, the pore surfaces are significantly influenced. The larger the suction, the greater the roughness of the pore surfaces.

The relationship between fractal dimension and suction of compacted loess is illustrated in Fig. 10. It can be observed that the fractal dimension of compacted loess shows a good linear relationship with the logarithm of suction, and the deviation parameter is greater than 0.91. It is similar to the fractal dimension variation of compacted loess during shearing (Xiao et al. 2022). The difference is that the fractal dimension increases linearly with the increase of axial strain during shearing; while during drying, the fractal dimension increases linearly with the logarithm of suction. Sun et al. (2020) also found that the fractal dimension of compacted bentonite increases with the increase of suction. In addition, they observed from the ESEM images with large magnifications that the roughness of the pore surfaces exactly increases with the increase of suction. However, Sun et al. (2020) did not provide the relationship between suction and fractal dimension due to the limited data. However, Gao et al. (2020) investigated the variation of fractal dimension of Zhaotong lignite during drying and drew an opposite conclusion; they reported that the fractal dimension decreases with the increase of suction. It might be because they dried the specimens under 200 ℃ and 280 ℃; the high temperature may lead to a variety of physical and chemical reactions in the Zhaotong lignite studied, so that the molecules are arranged directionally, hence reducing the roughness of the pore surfaces, i.e., the fractal dimension decreases with the increase of suction.

By comparing Fig. 11b, d, it can be found that under the same level of suction, the larger the compaction degree of compacted loess, the larger the fractal

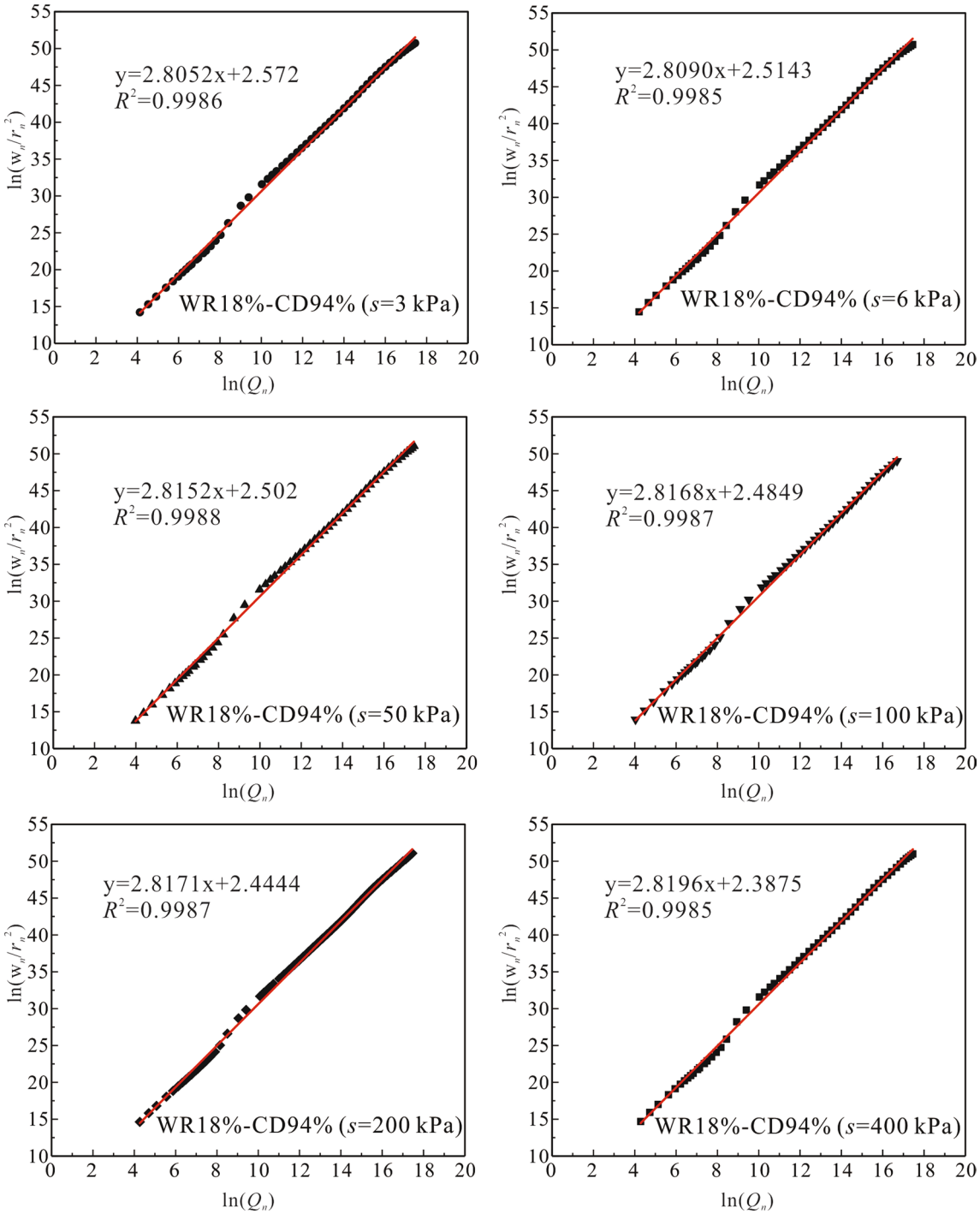

Fig. 10 Determination of the fractal dimension

dimension. This is similar to the fractal dimension variation of compacted loess with axial strain during shearing. For the shear shrinkage situation, it is known that the increase in axial strain is similar to the increase in dry density. Hence, it could be inferred that the fractal dimension increases with the shrinkage of specimens.

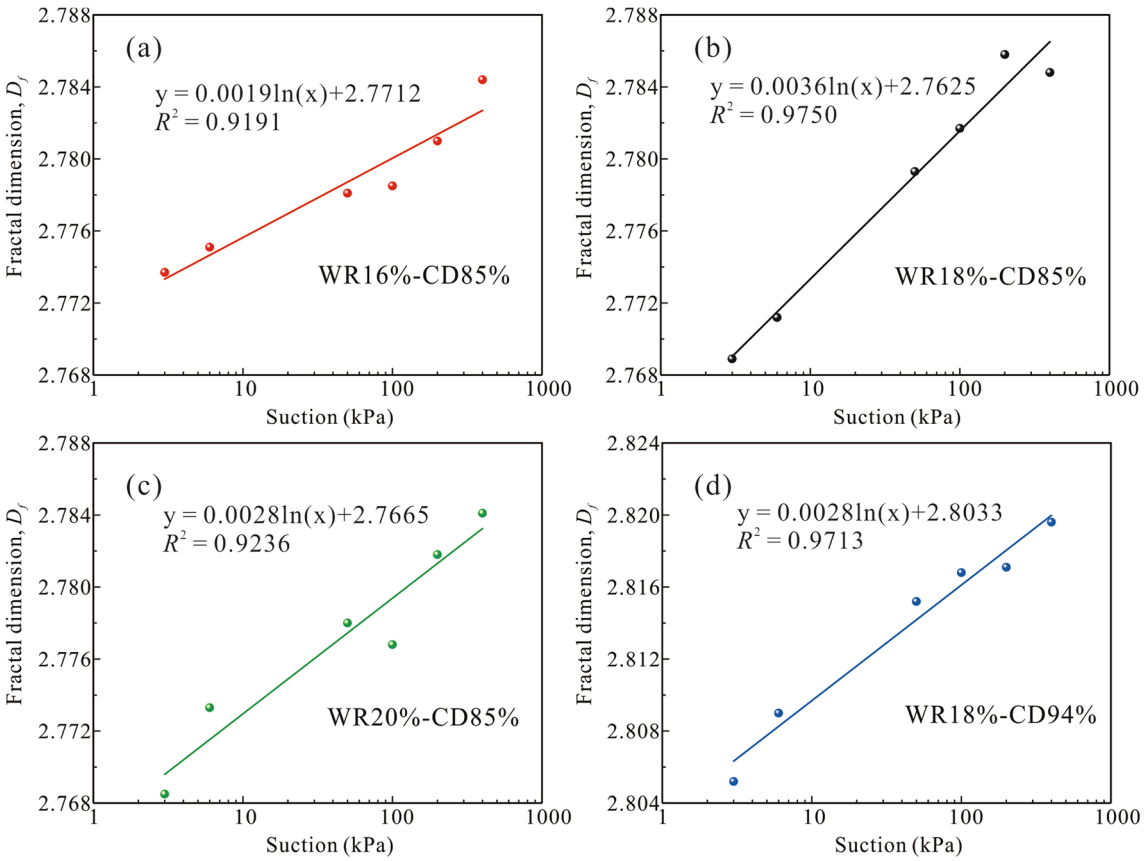

Fig. 11 Relationship between fractal dimension and suction of compacted loess: **a** WR16%-CD85%; **b** WR18%-CD85%; **c** WR20%-CD85%; **d** WR18%-CD94%

Conclusions

In this study, the SWCCs of compacted loess specimens with different initial microstructures are determined, and the microstructural evolution of compacted loess during drying is investigated. The main conclusions are as follows:

1. Molding water content and compaction energy influence the initial microstructure as well as the water retention capacity of compacted loess. Molding water content mainly affects the densities of macropores and mesopores, and compaction energy only affects the density of macropores. In addition, the microstructural state variable, ξ_m, increases with the increase of compaction energy at any molding water content, while ξ_m hardly changes with molding water content.
2. The AEV decreases with the increase of compaction energy, and compaction energy has little effect on the water retention capacity of compacted loess when suction exceeds 30 kPa. As the molding water content range of 16% to 20%, the AEV also reduces with the increase of molding water content, and the SWCCs of compacted loess specimens with the same compaction energy intersect at a suction, the specimen with a lower molding water content has a larger desorption rate than the specimen with a higher molding water content.
3. Changes in the PSD of compacted loess due to drying or suction increase are not significant. However, the fractal dimension of compacted loess shows a good linear relationship with the logarithm of suction, the larger the suction, the greater the fractal dimension, indicating that the roughness of the pore surfaces increases in response to suction increase during drying.

Acknowledgements

All authors would like to acknowledge the National Natural Science Foundation of China, the China Postdoctoral Science Foundation, and the Shaanxi Key Laboratory of Loess Mechanics and Engineering.

Author contributions

T.X.—Design and operation of the experiment, data collection and analysis, figure preparation, manuscript writing. P.L.—Data analysis, manuscript writing

and revision. Z.P.—Operation of the experiment. J.W.—Supervision. All authors read and approved the final manuscript.

Funding
This study was supported by the National Natural Science Foundation of China (42007251, 42027806), the China Postdoctoral Science Foundation (2019M653883XB), and the Shaanxi Key Laboratory of Loess Mechanics and Engineering (LME201803).

Availability of data and materials
The data used and analyzed in this study are available and can be provided by the corresponding author upon request.

Declarations

Competing interests
The authors declare that they have no competing financial interests.

Author details
[1]State Key Laboratory of Continental Dynamics, Department of Geology, Northwest University, Xi'an 710069, China. [2]Water Cycle and Geological Environment Observation and Research Station for the Chinese Loess Plateau, Ministry of Education, Zhengning 745399, China.

Received: 27 July 2022 Accepted: 8 December 2022
Published online: 22 December 2022

References

Alonso EE, Pinyol NM, Gens A (2013) Compacted soil behaviour: initial state, structure and constitutive modelling. Géotechnique 63(6):463–478. https://doi.org/10.1680/geot.11.P.134

Birle E, Heyer D, Vogt N (2008) Influence of the initial water content and dry density on the soil–water retention curve and the shrinkage behavior of a compacted clay. Acta Geotech 3:191–200. https://doi.org/10.1007/s11440-008-0059-y

Cai GQ, Zhou AN, Liu Y, Xu RZ, Zhao CG (2020) Soil water retention behavior and microstructure evolution of lateritic soil in the suction range of 0–286.7 MPa. Acta Geotech 15:3327–3341. https://doi.org/10.1007/s11440-020-01011-w

Cheng Q, Zhou C, Ng CWW, Tang CS (2020a) Thermal effects on water retention behavior of unsaturated collapsible loess. J Soil Sediment 20:765–762. https://doi.org/10.1007/s11368-019-02451-y

Cheng Q, Tang CS, Zeng H, Zhu C, An N, Shi B (2020b) Effects of microstructure on desiccation cracking of a compacted soil. Eng Geol 265:105418. https://doi.org/10.1016/j.enggeo.2019.105418

Chertkov VY (2000) Using surface crack spacing to predict crack network geometry in swelling soils. Soil Sci Soc Am J 64(6):1918–1921. https://doi.org/10.2136/sssaj2000.6461918x

Dijkstra T, Wasowski J, Winter M, Meng X (2014) Introduction to geohazards of Central China. Q J Eng Geol Hydrogeol 47:195–199. https://doi.org/10.1144/qjegh2014-054

Feng L, Zhang MS, Jin Z, Zhang SS, Sun PP, Gu TF, Liu XB, Lin H, An ZS, Peng JB, Guo L (2021) The genesis, development, and evolution of original vertical joints in loess. Earth Sci Rev 241:1033526. https://doi.org/10.1016/j.earscirev.2021.103526

Fu XL, Shao MA, Lu DQ, Wang HM (2011) Soil water characteristic curve measurement without bulk density changes and its implications in the estimation of soil hydraulic properties. Geoderma 167–168:1–8. https://doi.org/10.1016/j.geoderma.2011.08.012

Gao MQ, Ji PC, Miao ZY, Wan KJ, He QQ, Xue SW, Pei Z (2020) Pore structure evolution and fractal characteristics of Zhaotong lignite during drying. Fuel 267:117309. https://doi.org/10.1016/j.fuel.2020.117309

Gao QF, Zeng L, Shi ZN (2021a) Effects of desiccation cracks and vegetation on the shallow stability of a red clay cut slope under rainfall infiltration. Comput Geotech 140:104436. https://doi.org/10.1016/j.compgeo.2021.104436

Gao Y, Li Z, Sun DA, Yu HH (2021b) A simple method for predicting the hydraulic properties of unsaturated soils with different void ratios. Soil Tillage Res 209:104913. https://doi.org/10.1016/j.still.2020.104913

Gibbs HJ, Holland JL (1960) Subsidence characteristics of low-density silty soils in areas of Upper Meeker Canal-Missouri River basin project and lateral PE 41.2 Columbia basin project: Denver, Colorado, US Bureau of Reclamation, Division of Engineering Laboratory. Earth Laboratory Report No. EM-608

Hou XK, Qi SW, Li TL, Guo SF, Wang Y, Li Y, Zhang LX (2020) Microstructure and soil-water retention behavior of compacted and intact silt loess. Eng Geol 277:105814. https://doi.org/10.1016/j.enggeo.2020.105814

Huang M, Fredlund D, Fredlund M (2010) Comparison of measured and PTF predictions of SWCCS for loess soils in China. Geotech Geol Eng 28:105–117. https://doi.org/10.1007/s10706-009-9284-x

Jiang Y, Chen W, Wang G, Sun G, Zhang FY (2017) Influence of initial dry density and water content on the soil–water characteristic curve and suction stress of a reconstituted loess soil. Bull Eng Geol Environ 76:1085–1095. https://doi.org/10.1007/s10064-016-0899-x

Li LC (2021) An experimental study on soil water retention characteristics and rainfall infiltration characteristics of the compacted soils. Doctor Thesis, Chang'an University, Xi'an, China

Li P, Vanapalli SK, Li TL (2016) Review of collapse triggering mechanism of collapsible soils due to wetting. J Rock Mech Geotech 8:256–274. https://doi.org/10.1016/j.jrmge.2015.12.002

Li P, Shao SJ, Vanapalli SK (2020a) Characterizing and modeling the pore-size distribution evolution of a compacted loess during consolidation and shearing. J Soil Sediment 20:2855–2867. https://doi.org/10.1007/s11368-020-02621-3

Li YR, Zhang WW, He SD, Aydin A (2020b) Wetting-driven formation of present-day loess structure. Geoderma 377:114564. https://doi.org/10.1016/j.geoderma.2020.114564

Muñoz-Castelblanco J, Pereira J, Delage P, Cui Y (2012) The water retention properties of a natural unsaturated loess from northern France. Géotechnique 62:95–106. https://doi.org/10.1680/geot.9.P.084

Nan JJ, Peng JB, Zhu FJ, Ma PH, Liu R, Leng YQ, Meng ZJ (2021) Shear behavior and microstructural variation in loess from the Yan'an area. China Eng Geol 280:105964. https://doi.org/10.1016/j.enggeo.2020.105964

Ng CWW, Sadeghi H, Jafarzadeh F (2016a) Compression and shear strength characteristics of compacted loess at high suctions. Can Geotech J 54(5):690–699. https://doi.org/10.1139/cgj-2016-0347

Ng CWW, Sadeghi H, Hossen SB, Chiu CF, Alonso EE (2016b) Water retention and volumetric characteristics of intact and recompacted loess. Can Geotech J 53:1258–1269. https://doi.org/10.1139/cgj-2015-0364

Romero E, Gens A, Lloret A (1999) Water permeability, water retention, and microstructure of unsaturated compacted Boom clay. Eng Geol 54(1–2):117–127. https://doi.org/10.1016/S0013-7952(99)00067-8

Sreedeep S, Singh DN (2006) Methodology for determination of osmotic suction of soils. Geotech Geol Eng 24(5):1469–1479. https://doi.org/10.1007/s10706-005-1882-7

Sun HQ, Mašín DN, Najser JN, Neděla VM, Navrá TE (2020) Fractal characteristics of pore structure of compacted bentonite studied by ESEM and MIP methods. Acta Geotech 15(6):1655–1671. https://doi.org/10.1007/s11440-019-00857-z

Tang CS, Zhu C, Cheng Q, Zeng H, Xu JJ, Tian BG, Shi B (2021) Desiccation cracking of soils: a review of investigation approaches, underlying mechanisms, and influencing factors. Earth Sci Rev 216:105386. https://doi.org/10.1016/j.earscirev.2021.103586

Tu H, Vanapalli SK (2016) Prediction of the variation of swelling pressure and one-dimensional heave of expansive soils with respect to suction using the soil-water retention curve as a tool. Can Geotech J 53:1213–1234. https://doi.org/10.1139/cgj-2015-0222

van Genuchten MT (1980) A closed-form equation for predicting the hydraulic conductivity of unsaturated soils. Soil Sci Soc Am J 44(5):892–898. https://doi.org/10.2136/sssaj1980.03615995004400050002x

Vanapalli SK, Fredlund DG, Pufahl DE, Clifton AW (1996) Model for the prediction of shear strength with respect to soil suction. Can Geotech J 33(3):379–392. https://doi.org/10.1139/t96-060

Vanapalli SK, Fredlund DG, Pufahl DE (1999) The influence of soil structure and stress history on the soil-water characteristics of a compacted till. Géotechnique 49:143–159. https://doi.org/10.1680/geot.1999.49.2.143

Wang YG, Zhang AJ, Ren WY, Niu LS (2019) Study on the soil water characteristic curve and its fitting model of Ili loess with high level of souble salts. J Hydrol 578:124067. https://doi.org/10.1016/j.jhydrol.2019.124067

Xiao T, Li P, Shao SJ (2022) Fractal dimension and its variation of intact and compacted loess. Powder Technol 395:476–490. https://doi.org/10.1016/j.powtec.2021.09.069

Xu PP, Zhang QY, Qian H, Qu WG, Li MN (2021) Microstructure and permeability evolution of remolded loess with different dry densities saturated seepage. Eng Geol 282:105875. https://doi.org/10.1016/j.enggeo.2020.105875

Ye YX, Zou WL, Han Z, Liu XW (2019) Predicting the entire soil-water characteristic curve using measurement within low suction range. J Mt Sci 16:17. https://doi.org/10.1007/s11629-018-5233-6

Ying Z, Cui YJ, Benahmed N, Duc M (2021) Investigating the salinity effect on water retention property and microstructure changes along water retention curves for lime-treated soil. Constr Build Mater 303:124564. https://doi.org/10.1016/j.conbuildmat.2021.124564

Zhang BQ, Li SF (1995) Determination of the surface fractal dimension for porous media by mercury porosimetry. Ind Eng Chem Res 34(4):1383–1386. https://doi.org/10.1021/ie00043a044

Zhang FY, Yan BB, Feng XM, Lan HX, Kang C, Lin X, Zhu XS, Ma WG (2019) A rapid loess mudflow triggered by the check dam failure in a bulldoze mountain area, Lanzhou, China. Landslides 16:1981–1992. https://doi.org/10.1007/s10346-019-01219-2

Zhang FY, Zhao CX, Lourenço SDN, Dong S, Jiang Y (2021) Factors affecting the soil–water retention curve of Chinese loess. Bull Eng Geol Environ 80:717–729. https://doi.org/10.1007/s10064-020-01959-9

Zhang HX, Zeng RQ, Zhang Y, Zhao SF, Meng XM, Li YX, Liu WC, Meng XP, Yang YP (2022) Subsidence monitoring and influencing factor analysis of mountain excavation and valley infilling on the Chinese Loess Plateau: a case study of Yan'an New District. Eng Geol 297:106482. https://doi.org/10.1016/j.enggeo.2021.106482

Zhao Y, Cui YJ, Zhou H, Feng XT, Huang ZQ (2017) Effects of void ratio and grain size distribution on water retention properties of compacted infilled joint soils. Soil Found 57:50–59. https://doi.org/10.1016/j.sandf.2017.01.004

Zhu CH, Li N (2019) Ranking of influence factors and control technologies for the post-construction settlement of loess high-filling embankments. Comput Geotech 118:103320. https://doi.org/10.1016/j.compgeo.2019.103320

Publisher's Note